LOI12-15-003

Measurement of the Ratio G_E^n/G_M^n by the Double-polarized $^2H(\overrightarrow{e}, e'\overrightarrow{n})$ Reaction

a Letter of Intent to Jefferson Lab. PAC 43.

May 16, 2015

J.R.M. Annand[1], D.J. Hamilton, K. Hamilton, D. Ireland, K. Livingston, I.J.D. MacGregor, B. Seitz, D. Sokhan
University of Glasgow, Glasgow G12 8QQ, UK.

B. Wojtsekhowski, A. Camsonne, J.P. Chen, J. Gomez, O. Hansen, D. Higinbotham, M. Jones, C. Keppel, R. Michaels
Thomas Jefferson National Accelerator Facility, Newport News, VA 23606, USA.

N. Piskunov, S. Basylev, O. Gavrishchuk, D. Kirillov, G. Meshcheryakov, J. Mushinsky, A. Nagaytsev, I. Savin, I. Slepnev, V. Slepnev, I. Sitnik
Joint Institute for Nuclear Research, Dubna, Russian Federation.

V. Bellini, P. Castorina, F. Mammoliti, M.L. Sperduto, C.M. Sutera and F. Tortorici
INFN Catania and University of Catania, Catania, Italy.

Abstract

We propose a measurement of double polarized $^2H(\overrightarrow{e}, e'\overrightarrow{n})$ at values of $Q^2 = 2.0, 4.0, 6.0, 9.3\ (GeV/c)^2$. The ratio of electric to magnetic elastic form factors G_E^n/G_M^n will be extracted from the ratio of transverse and longitudinal components of the spin polarization P_x/P_z, which is transferred to the recoiling neutron from an incident, longitudinally polarized electron. The experiment will be performed in Hall-A of Jefferson Laboratory, utilizing several of the common components of the Super BigBite apparatus. The neutron polarimeter consists of a custom array of plastic scintillator blocks (the analyzer) and the hadron calorimeter HCAL to measure the azimuthal modulation in neutron scattering. The geometry is suitable to detect charge-exchange $n-p$ scattering, as well as standard $n-p$, which provides a large gain in analyzing power for incident neutron momenta above ~ 3 GeV/c. This results in a large increase in the polarimeter's figure of merit (a factor ~ 10 at an incident momentum of 5.8 GeV/c) which has brought Q^2 values as high as 9.3 $(GeV/c)^2$ within reach of a recoil polarimetry experiment

[1]Corresponding author: john.annand@glasgow.ac.uk

Contents

1 Introduction

The understanding of nucleon structure and the nature of quark confinement is one of the central goals facing nuclear physics today. At the $\sim fm$ scales typical of hadrons, quantum chromodynamics (QCD), the field theory describing the quark-gluon interaction, is too strong to be solved by perturbative methods (pQCD) and the understanding of non-perturbative QCD remains a pivotal problem of theoretical physics.

One of the critical factors driving progress in understanding nucleon structure is the availability of high precision electron scattering results over a broad range of Q^2. The higher Q^2 domain is relatively unexplored and thus has immense potential to assess different nucleon structure models. Elastic form factors remain a major source of information about quark distributions at small transverse distance scales and the Q^2 dependence of $\mathrm{G_E^p/G_M^p}$ has generated more theoretical papers than any other result to come out of Jefferson Laboratory (JLab). There is considerable anticipation regarding new results that push both $\mathrm{G_E^p/G_M^p}$ and $\mathrm{G_E^n/G_M^n}$ to higher values of Q^2.

The Super-Bigbite-Spectrometer (SBS) experimental program has three approved measurements of nucleon elastic form factors [1, 2, 3]. In addition E12-07-108 [4] will measure G_M^p up to 17.5 $(\mathrm{GeV/c})^2$, using the Hall-A HRS spectrometers to achieve a 1-2% measurement of the $e-p$ elastic scattering cross section. Thus extraction of absolute values of G_M^n, G_E^p and G_E^n from ratio measurements will be possible. A major strength of the program in Hall-A is the ability to measure all four of the Electromagnetic Form Factors (EMFF), with sufficient accuracy and reach in Q^2 to address some of the most fundamental and topical questions in hadronic physics.

We propose to measure $\mathrm{G_E^n/G_M^n}$ to high precision over a range of $\mathrm{Q}^2 = 2.0 - 9.3$ $(\mathrm{GeV/c})^2$, by quasi-elastic $^2\mathrm{H}(\vec{\mathrm{e}},\mathrm{e}'\vec{\mathrm{n}})$. This will overlap in kinematic range with published data [5] and the new experiment E12-09-016 [1], both of which employ $^3\overrightarrow{He}(\vec{\mathrm{e}},\mathrm{n})$. Existing $^2\mathrm{H}(\vec{\mathrm{e}},\mathrm{e}'\vec{\mathrm{n}})$ data [6] extend up to $\mathrm{Q}^2 = 1.5$ $(\mathrm{GeV/c})^2$ only. Neutron measurements are technically very challenging and must employ quasi-free scattering from light nuclei, which introduces some uncertainty in extrapolation to the free-neutron case, but generally is more straightforward for ^{2}H compared to ^{3}He. Employing different experimental techniques, with different systematic effects, and different nuclear targets, with different binding and final state interaction effects provides an extremely valuable cross check on the accuracy of the measurements.

1.1 Physics Motivation

The EMFF are among the simplest of hadron-structure observables, but none the less they continue to play a vital role in constraining non-perturbative QDC treatments of nucleon structure. They also provide an indispensable constraint to Generalized Parton Distribution (GPD) analyses to extract the "3D" structure of the nucleon. In the one-photon exchange approximation the most general form of a relativistically covariant hadronic current for a spin-1/2 nucleon, which satisfies current conservation, is:

$$J^{\mu}_{hadronic} = e\bar{N}(p')\left[\gamma^{\mu}F_1(Q^2) + \frac{i\sigma^{\mu\nu}q_{\nu}}{2M}F_2(Q^2)\right] \tag{1}$$

where $\bar{N}(p')$ is the nucleon Dirac spinor for the final momentum p', and $F_1(Q^2)$ and $F_2(Q^2)$ are the Dirac (helicity conserving) and Pauli (helicity flip) form factors. It is often convenient to express cross sections and other observables in terms of the Sachs electric (G_E) and magnetic (G_M) form factors which are linear combinations of F_1 and F_2.

$$G_E = F_1 - \tau F_2 \qquad G_M = F_1 + F_2 \tag{2}$$

where $\tau = Q^2/4M_N^2$. G_E and G_M represent, in the Breit frame, the Fourier transforms of the distributions of charge and magnetic moment respectively of the nucleon constituents.

1.1.1 The scaling behavior of EMFF and non-perturbative QCD

At sufficiently high values of Q^2, F_1 is expected to scale as $1/Q^4$, while F_2 should scale as $1/Q^6$ [7], essentially on the basis of quark counting rules. After publication of Ref.[8], it became clear that F_2^p/F_1^p did not scale as $1/Q^2$, as evident in Fig.1 A. The difference in apparent scaling behavior of proton data derived from double-polarized measurements [8, 9, 10, 11, 12], as opposed to Rosenbluth separation of differential cross sections [13, 14, 15], is now thought to be due to two-photon exchange effects. Rosenbluth separation is highly sensitive to two-photon exchange effects, while double-polarized measurements are relatively insensitive.

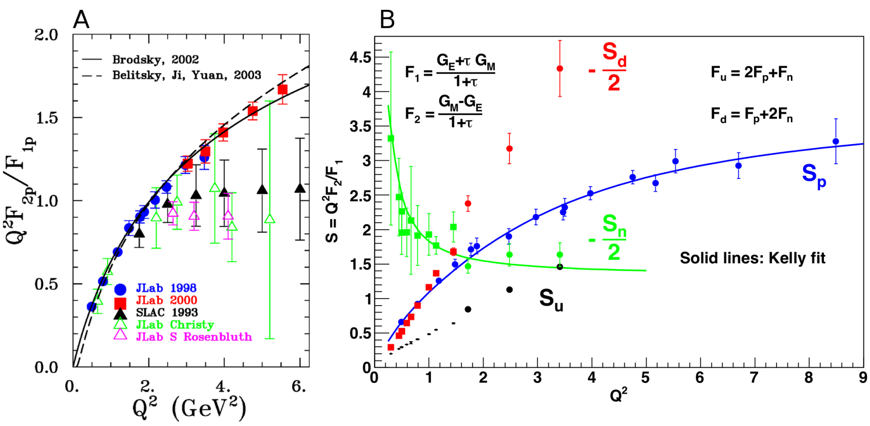

Figure 1: Q^2F_2/F_1 as a function of Q^2. A: proton data derived from world double polarized measurements (red, blue) and Rosenbluth separation (green, magenta, black) compared to the theoretical predictions of Ref.[16]. B: the fit of [18] to proton (blue) and neutron (green) world data. Also shown is a flavor decomposition with u (black) and d (red).

A subsequent pQCD calculation [16] has relaxed the assumption [7] that the quarks move collinearly with the proton. It included components in the light-cone nucleon wave functions with a quark orbital angular momentum projection $\mathrm{L_z} = 1$. This is equivalent to relaxing hadron helicity conservation and produces the scaling relation $F_2/F_1 \propto \ln^2(Q^2/\Lambda^2)/Q^2$, where Λ is a non-perturbative mass scale. Agreement with the JLab double polarized $\mathrm{G_E^p/G_M^p}$ measurements is quite good up to about 6 $(\mathrm{GeV/c})^2$ although newer data, at higher Q^2, suggest a more gradual fall off with Q^2. The implication of this scaling is that quark orbital angular momentum is playing an important dynamical role in the Q^2-evolution of the proton form factors. Fig.1 B [17] displays both proton and neutron results from JLab, along with an empirical fit to the data [18]. Neutron behavior is quite different from the proton, but obviously the neutron data span a much smaller range of Q^2. This LOI proposes to expand the range of Q^2 by a factor ~ 3 for $\mathrm{G_E^n/G_M^n}$, up to 9.3 $(GeV/c)^2$.

QCD-compatible calculations of baryon structure use constituent quarks as the relevant degrees of freedom and one theoretical technique has come to prominence in the past decade, based on the infinite series of Dyson-Schwinger Equations (DSE) that interrelate the Green's functions of QCD [19]. Recent calculations explicitly describe the dynamical generation of the mass of constituent quarks, and show excellent agreement with lattice QCD results. Using the dressed quarks as the elementary degrees of freedom, the nucleon form factors may be calculated using a Poincaré covariant Faddeev equation (DSE/F) [20]. While still an approximation, the DSE/F approach is based on first principles. It is limited, however, in that precisely three constituent quarks are considered, so that for instance pion-cloud effects are not investigated. However, it is reasonable to assume the dominance of the 3-quark component of the wave function at relatively high values of Q^2.

Building on the work of Ref.[20] a unified study of nucleon and Δ elastic and transition form factors has recently been made [21], which the authors have dubbed a "QCD-kindred framework". This framework evidently (Fig. 2) provides a consistent and reasonable description of both $\mu_p G_E^p/G_M^p$ and $\mu_n G_E^n/G_M^n$ and predicts for both a zero-crossing point. The location of the zero crossing point (if any) of the ratios has implications for the location and width of the transition region between constituent- and parton-like behavior of the dressed quarks. A more rapid transition from non-perturbative to perturbative behavior pushes the proton zero point to higher Q^2,while conversely the neutron zero point is pushed to lower Q^2. Thus the ability of the JLab EMFF measurements to push into the $Q^2 \sim 10\ (GeV/c)^2$ domain will have a major impact on the development of non-perturbative QCD. In the case of the neutron the kinematic region of interest is completely unexplored.

Within the QCD-kindred framework [21] di-quark correlations are behind the zero-crossing behavior of G_E/G_M. Measurements of all four Sachs form factors, provide the means to make a flavor separation to the Dirac and Pauli form factors of the u and d quarks: $F^u_{1,2}$, $F^d_{1,2}$ respectively. Assuming negligible nucleon strange content they are linear combinations of the proton and neutron form factors:

$$F^u_{1,2}(Q^2) = F^n_{1,2} + 2F^p_{1,2} \qquad F^d_{1,2}(Q^2) = 2F^n_{1,2} + F^p_{1,2} \tag{3}$$

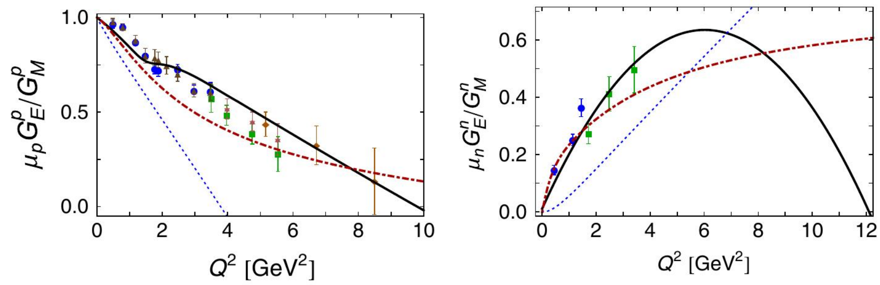

Figure 2: Left: QCD-kindred calculation [21] (black line) of $\mu_p \mathrm{G_E^p}/\mathrm{G_M^p}$ compared to JLab data [8, 9, 10, 11, 12]. Right: equivalent calculation of $\mu_n \mathrm{G_E^n}/\mathrm{G_M^n}$ (black line) compared to JLab. data [5, 6]. Red dot-dash lines are from Ref. [18], and blue dotted lines from Ref. [22].

This emphasizes the importance of measuring both proton and neutron distributions. A recent Hall-A publication [23] shows an intriguing difference in scaling behavior between the u and d quarks. Above ~ 1 (GeV$/c)^2$, $F^d_{1,2}$ appears to scale roughly as $1/Q^4$, whereas $F^u_{1,2}$ appears to scale roughly as $1/Q^2$.

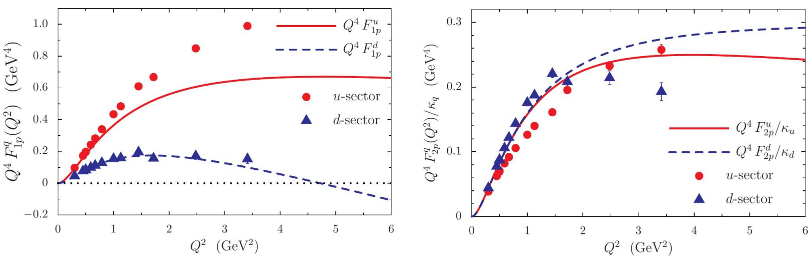

Figure 3: Left: Scaling behavior of F_1 and F_2 for u and d quarks. Data from Ref. [23], curves from the NJL calculation of Ref. [24]

This behavior is addressed in Ref. [21] and also in a calculation made within the framework of a covariant, confining Nambu-Jona-Lasinio (NJL) model [24]. For F_1 the dominance of the u-quark sector is interpreted as a consequence of scalar di-quark correlations, which play a smaller role in the d-quark sector. The u-d difference for F_2 is less dramatic, due to axial-vector diquark and pion-cloud contributions to the d sector, counteracting the effect of the scalar di-quark correlation. The comparison with data is limited to $Q^2 \leq 3.5\,(GeV/c)^2$, above which there is no data on G^n_E. Precise new neutron data at $Q^2 > 3.5\,(GeV/c)^2$ and confirmation of the behavior at $1.5 < Q^2 < 3.5\,(GeV/c)^2$ are required to further these new theoretical developments.

1.1.2 The link with Generalized Parton Distributions

Generalized Parton Distributions (GPD) describe correlations between spatial and momentum degrees of freedom and permit the construction of various types of “3-D images" of the nucleon. The nucleon elastic form factors are critical to the experimental determination of GPDs [25]. In Deeply Virtual Compton Scattering (DVCS), which is generally held to be the optimum channel to access GPD information, the interference between Bethe Heitler and DVCS Handbag mechanisms is measured and the separation of these amplitudes requires EMFF information. The first moments of GPDs are related to the elastic form factors through model independent sum rules:

$$\int_{-1}^{+1} dx H^q(x,\xi,Q^2) = F_1^q(Q^2) \qquad \int_{-1}^{+1} dx E^q(x,\xi,Q^2) = F_2^q(Q^2) \tag{4}$$

These relations are currently some of the most important constraints on the forms of the GPD's and, since it is extremely unlikely that the GPDs will be mapped out exhaustively in the near future, constraints such as those in Eq.4 will be critical to their practical determination. Already the constraints from Eq.4 have played an important role in the first estimates of nucleon quark angular momentum using the Ji Sum Rule and constraining GPDs is in itself an excellent reason to experimentally determine the nucleon elastic form factors.

1.2 Previous Form Factor Measurements

1.2.1 Polarized Target

Vector Polarized $^2\mathbf{H}$ has the neutron and proton spins aligned in parallel and measurements with such a polarized neutron-proton target have been made at $\mathrm{Q}^2 = 0.21$ [26] and 0.495 (GeV/c$^{2)}$ [27]. Polarized ^{3}He has the advantage that $\sim 90\%$ of the nuclear polarization is carried by the neutron. At Mainz, polarized ^{3}He target measurements have taken place at $\mathrm{Q}^2 = 0.385$ (GeV/c)^2 [28], at 0.385 (GeV/c)^2 [29] and at 1.5 (GeV/c)^2 [30]. In the GEn(1) experiment at JLab [5] the high beam energy, high performance ^{3}He target and large acceptance detectors has enabled the Q^2 range to be extended up to 3.4 (GeV/c)^2.

1.2.2 Recoil Polarimetry

There have been several experiments to measure $\mathrm{G_E^n/G_M^n}$ by recoil polarimetry. Proof-of-principle measurements at MIT-Bates [31] were followed by more quantitative measurements at Mainz, firstly within collaboration A3 [32, 33] and subsequently within collaboration A1 [34]. While the Mainz program was still in progress, experiments at JLab started to come online, and Hall-C measurements of $\mathrm{G_E^n/G_M^n}$ have been published at Q^2 of 0.5 and 1.0 (GeV/c)^2 [35] and 1.45 (GeV/c)^2 [6], which is currently the highest value of Q^2 measured by recoil polarization.

1.3 New EMFF Measurements at JLab.

Measurement of the nucleon EMFF will be a major component of Hall-A experimental programme. The SBS project has three approved measurements: $\mathrm{G_E^n/G_M^n}$ [1], $\mathrm{G_M^n/G_M^p}$ [2] and $\mathrm{G_E^p/G_M^p}$ [3]. These three measurements, together with a very precise measurement of $\mathrm{G_M^p}$ [4] in Hall A using the HRS Spectrometers, will collectively determine all four nucleon form factors with unprecedented reach in $\mathrm{Q^2}$ and accuracy.

E12-09-016: *Measurement of the Neutron Electromagnetic Form Factor Ratio* $\mathrm{G_E^n/G_M^n}$ *at high* $\mathrm{Q^2}$ [1]. This experiment (GEn(2)), will measure the double-spin asymmetry in quasi-elastic $\overrightarrow{^3He}(\overrightarrow{e},\mathrm{e'n})\mathrm{pp}$ using a new highly-polarized ^{3}He target, capable of withstanding high beam currents. The scattered electron will be detected in BigBite and the recoiling neutron in HCAL. Measurements are proposed at $\mathrm{Q^2} = 1.5$, 3.7, 6.8, 10.2 $\mathrm{(GeV/c)^2}$, which can be compared to the current highest GEn(1) point at $\mathrm{Q^2} = 3.4\ \mathrm{(GeV/c)^2}$. New $\mathrm{G_E^n/G_M^n}$ data will have enormous physics impact and, given that neutron measurements are extremely challenging, confirmation of these results by the present, different experimental technique will be extremely important.

E12-09-019: *Precision Measurement of the Neutron Magnetic Form Factor up to* $Q^2 = 13.5\ (GeV/c)^2$ [2]. In experiment E12-09-019 the combination of high precision measurements of $\mathrm{G_M^p}$ and $\mathrm{G_M^n}$ will permit the reconstruction of the individual u and d quark distributions with an impact-parameter resolution of 0.05 fm. These data are needed both to determine the $u - d$ difference and to study the QCD mechanisms which govern these distributions. G_M^n will be obtained from the cross-section ratio of $^2\mathrm{H(e,e'n)}$ and $^2\mathrm{H(e,e'p)}$ quasi-free scattering from the deuteron. This ratio method has also been proposed using CLAS12, which can measure on a fine grid of $\mathrm{Q^2}$ points. However, the SBS measurement can be made at much higher luminosity and can achieve superior precision at high $\mathrm{Q^2}$. The HCAL calorimeter for the SBS measurement offers very similar proton and neutron detection efficiencies which are close to 100%. This largely eliminates a potential major source of systematic uncertainty in the ratio method.

E12-07-109: *Large Acceptance Proton Form Factor Ratio Measurements at High* Q^2 *using the Recoil Polarization Method [3].*
This experiment will measure the ratio $\mathrm{G_E^p/G_M^p}$ at $\mathrm{Q^2} = 5, 8, 12\ \mathrm{(GeV/c)^2}$ with a relative uncertainty of ~ 0.1, which should answer the question as to where in Q^2 the ratio crosses zero, if at all. The experiment will use the 11 GeV polarized electron beam, a 40 cm long liquid hydrogen target, the BigCal electromagnetic calorimeter to detect the elastically scattered electrons and SBS, equipped as a polarimeter, for the detection of the recoiling proton. A luminosity of $\sim 10^{39}$ will be necessary to reach the desired precision, and the technical solutions to the problems imposed by high rates in the detectors will be of general benefit to the SBS programme.

E12-07-108: *Precision measurement of the Proton Elastic Cross Section at High* Q^2 [4]. This experiment uses the two Hall-A HRS to perform a high precision (2%) measurement of $H(e,e'p)$ at values of Q^2 up to 17.5 $(GeV/c)^2$. Commissioning of this experiment has already commenced and the data will yield high precision values of G_M^p.

E12-11-009: *The Neutron Electric Form Factor at Q^2 up to $7\,(GeV/c)^2$ from the Reaction $^2H(\overrightarrow{e}, e'\overrightarrow{n})$ via Recoil Polarimetry* [36]. This measurement of $\mathrm{G_E^n/G_M^n}$ has been proposed for Hall-C using the Super High Momentum Spectrometer and a custom built neutron polarimeter. The polarimeter registers $n-p$ interactions in a series of segmented plastic-scintillator analyzers and detects recoiling protons in top and bottom, segmented arrays of $\delta E - E$ counters. With this geometry it is not possible to detect charge-exchange $n-p$ scattering which produces a much higher analyzing power at neutron momenta above ~ 3 GeV/c. Thus this polarimeter will have a relatively low figure of merit for $Q^2 \gtrsim 4\,(GeV/c)^2$, as discussed in Sec.2.1.3.

2 Double-Polarized Measurements of G_E/G_M

The double polarization method for the measurement of G_E was originally proposed [37] to improve the experimental sensitivity to the spin-flip form factor $\mathrm{F_2}$ at large momentum transfer, and subsequent work [38] developed the formalism. A number of form-factor measurements have been performed in recent years: either with polarized nucleon targets, or with a polarimeter to measure the polarization transfer to the recoiling nucleon. The technique of choice depends on the comparison of achievable luminosity, detector efficiency, detector acceptance and the experimental asymmetry, which in turn depends on the target polarization or polarimeter analyzing power.

In the case of the neutron, quasi-elastic scattering from the neutron bound in ^{2}H or ^{3}He offers the nearest approximation to the free scattering case. Bound-nucleon and final-state-interaction effects become less important as momentum transfer increases, but none the less it is highly desirable to have data on both targets to check consistency. Neutron measurements are inherently more challenging than their proton equivalents, as demonstrated by their more restricted kinematic range $\mathrm{G_E^n/G_M^n}$: $\mathrm{Q^2} \leq 3.5$ (GeV/c)^2 as opposed to $\mathrm{G_E^p/G_M^p}$: $\mathrm{Q^2} \leq 8.5$ (GeV/c)^2 . A set of high precision measurements of $\mathrm{G_E^n/G_M^n}$ at $\mathrm{Q^2} = 2-9$ (GeV/c)^2 will have extremely high selectivity of the quite diverse predictions of different theoretical models. Thus it is extremely important to have reliable, independently verified neutron results.

Whether working with a polarized target or a recoil polarimeter, the ability to separate G_E from G_M and the relative freedom from two-photon exchange effects make double-polarization asymmetry measurements the techniques of choice for accessing G_E^n.

2.0.1 Polarized Beam and Recoil Polarimetry

For a free nucleon the polarization transferred from the electron to the nucleon can be written as:

$$P_x = -hP_e \frac{2\sqrt{\tau(1+\tau)}\tan\frac{\theta_e}{2} G_E G_M}{G_E^2 + \tau G_M^2 (1 + 2(1+\tau)\tan^2\frac{\theta_e}{2}} \quad (5)$$

$$P_y = 0 \quad (6)$$

$$P_z = hP_e \frac{2\tau\sqrt{1+\tau+(1+\tau)^2\tan^2\frac{\theta_e}{2}}\tan\frac{\theta_e}{2}G_M^2}{G_E^2+\tau G_M^2(1+2(1+\tau)\tan^2\frac{\theta_e}{2})} \tag{7}$$

$$\frac{P_x}{P_z} = \frac{1}{\sqrt{\tau+\tau(1+\tau)\tan^2\frac{\theta_e}{2}}} \cdot \frac{G_E}{G_M} \tag{8}$$

where h and P_e are the helicity and polarization respectively of the electron beam. Eq.8 requires the measurement of the longitudinal component of the neutron polarization P_z and this must be precessed into the transverse plane. The angle of precession through a magnetic field may be expressed as

$$\chi = \frac{2\mu_n}{\hbar c}\frac{1}{\beta_n}\int_L \mathbf{B}.dl \tag{9}$$

where $L(x, y, z)$ is the path through the field, $\mathbf{B} = (B_x, B_y, B_z)$ is the flux density, μ_n is the neutron magnetic moment and β_n is the neutron velocity. With a horizontal field $(B_x, 0, 0)$ the spin will precess in the $y - z$ plane (See Sec.2.1).

2.1 Nucleon Polarimetry

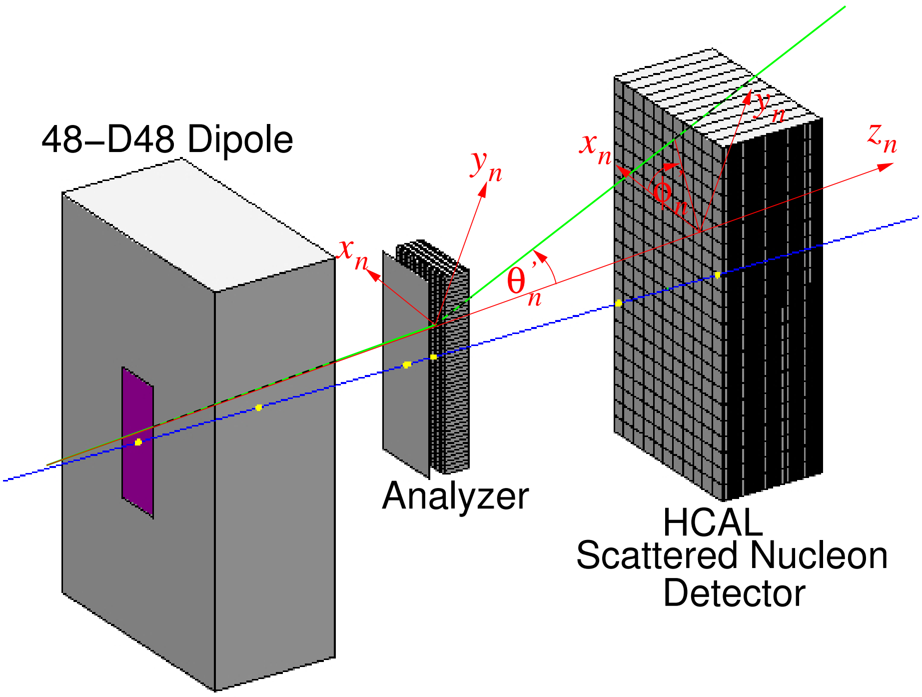

Figure 4: Schematic view of a neutron polarimeter, using SBS detector components

Nucleon polarimetry depends on the spin-orbit interaction of an incident nucleon with a target nucleon or nucleus, which produces an azimuthal modulation of the scattering process:

$$\sigma(\theta_n^{'}, \phi_n^{'}) = \sigma(\theta_n^{'}) \left[1 + A_y(\theta_n^{'}) \left\{P_x^n \sin\phi_n^{'} + P_y^n \cos\phi_n^{'}\right\}\right] \tag{10}$$

where $\sigma(\theta_n^{'})$ is the unpolarized scattering differential cross section, $A_y(\theta_n^{'})$ is the analyzing power of the scattering process and P_x^n, P_y^n are respectively the horizontal and vertical components of the incident nucleon polarization. Scattering angles are shown in Fig.4. The effectiveness of any polarimeter will depend on a combination of its detection efficiency and analyzing power, which can be parametrized as a figure of merit $\mathcal{F}$ given by:

$$\mathcal{F}^2(p_n) = \int \varepsilon(p_n, \theta_n^{'})\, A_y^2(p_n, \theta_n^{'}) d\theta_n^{'} \tag{11}$$

where $\varepsilon(p_n, \theta_n^{'})$ is the detection efficiency which depends on the cross section for the scattering process and the thickness of the polarimeter material. The angular range is determined by the polarimeter geometry and obviously good acceptance for the region where A_y is large is important. The thickness is usually limited in practice by multiple scattering considerations, as with multiple scattering the initial scattering plane is lost. If $\mathcal{F}$ is known then the precision of the obtained incident polarization may be obtained from:

$$\Delta P = \sqrt{\frac{2}{N_{inc}\mathcal{F}^2}} \tag{12}$$

where N_{inc} is the number of incident particles. Note that the present polarimeter (Fig. 4) has full azimuthal coverage up to polar angles of $\sim 15°$, which will contain most of the useful forward angle scattering. It is also advantageous for untangling the P_x and P_y polarization components.

2.1.1 Neutron analyzing power at several GeV/c

Neutron polarimetry using an organic analyzing material is generally based on free and quasi-free $n-p$ scattering processes, since the detected recoiling proton is used to reconstruct the scattering kinematics. By contrast, quasi-free $n-n$ scattering will produce a low-energy, recoiling charged ion which is difficult to detect. In comparison to proton polarimetry, the analyzing power A_y for neutron polarimetry is rather poorly known. Free $n-p$ scattering is in principle the best analyzer of neutron polarization, but the use of a hydrogen analyzer is challenging technically and scattering from C or CH_2 offers an easier solution, although A_y for quasi-free scattering is generally lower than the free-scattering case.

There is a proposal to measure neutron analyzing powers for organic materials using the polarized neutron beam at JINR Dubna [40], but this is unlikely to happen before late 2015. Thus we have analyzed the available experimental evidence (Sec. 2.1.2) in order to estimate of the neutron analyzing power.

2.1.2 Experimental data for polarized nucleon-nucleon scattering

Information on polarized nucleon scattering for incident momenta $p_N \gtrsim 1.5$ GeV/c is presented in Fig. 5 A. This comes from a number of sources.

1. Measurements of the asymmetries of the $d(\vec{p},p')n$ and $d(\vec{p},n)p$ processes have been performed in the 1970s [41, 42] which, in the case of the former, are consistent with elastic $\vec{p}+p \to p+p$ measurements [43]. These experiments measured both $p-p$ and $p-n$ scattering .
2. Inclusive measurements of $\vec{p}+\mathrm{CH_2} \to p+X$ [44], and $\vec{p}+\mathrm{C} \to p+X$ [45, 46] have been obtained in the calibration of proton polarimeters used at ANL, Dubna and JLab.
3. Measurements of the asymmetries of Charge Exchange n-p scattering (CE n-p) [47, 48], have also been made at ANL in the 1970s

It is immediately obvious (Fig. 5) that $p-n$ (equivalent to $n-p$) polarization is strongly dependent on incident nucleon momentum p_{lab}, as well as t. On the other hand CE n-p is t-dependent, with a large polarization at sufficiently large t, but has no apparent strong dependence on p_{lab}.

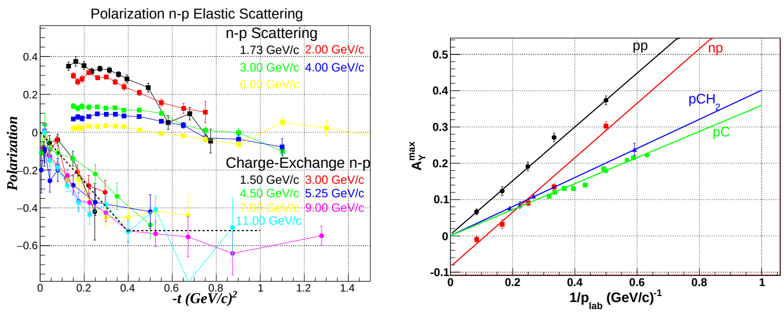

Figure 5: A: Comparison of the t-dependence of the polarization of $p-n$ [41, 42] and CE $n-p$ scattering [47, 48] for a range of incident momenta. B: The dependence of the maximum of A_Y on $1/p_{lab}$. Black circles: ANL $d(\vec{p},p')n$ data [41, 42]; black line: linear fit. Red squares: ANL $d(\vec{p},n)p$ data [41, 42]; red line: linear fit. Blue triangles [44]: $\vec{p}+\mathrm{CH_2} \to charged + X$; blue line: linear fit [44]. Green squares [45] and circles [46]: $\vec{p}+\mathrm{C} \to charged + X$; green line: linear fit [44].

Fig.5B displays the maximum values of the angle-dependent polarization asymmetries of $p-p$ and $p-n$ scattering, as determined from the data of Ref.[41, 42, 44, 45, 46] and plotted in as a function of $1/p_{lab}$. The main features are the negative offset of the $p-n$ data with respect to $p-p$ and the factor 2 reduction in analyzing power of quasi-free (^{12}C) with respect to free scattering.

2.1.3 The Figure of Merit for neutron polarimetry

For optimum FOM (Eq. 11) over a range of p_{lab} the polarimeter should be capable of detecting not only $n-p$ events, where the neutron scatters forward and the proton recoils sideways, but also charge-exchange $n-p$ where the incident neutron recoils sideways and the proton is knocked forward. The proposed polarimeter in this LOI (Sec. 3.2) has this capability, while the polarimeter of experiment E12-11-009 relies on detecting sideways recoiling protons and has no acceptance for charge-exchange $n-p$ scattering.

Quasi-free $p-p$ scattering has a factor-two reduction in A_Y compared to the free case and for $n-p$ the same reduction factor is consistent with the polarimeter analyzing power obtained in a previous JLab measurement of G_E^n/G_M^n [6]. To estimate the FOM we assume that this factor-two reduction also holds for quasi-free, CE $n-p$ scattering. Values of FOM are given in Fig. 6. They have been calculated by Monte Carlo, using differential free $n-p$ cross sections from the SAID partial wave analysis [49], multiplied by a factor for the effective number of protons in CH. Analyzing powers are based on the data in Fig. 5. An empirical fit [50] of the $n-p$ p_n, t-dependence was used, while for CE $n-p$ the relation $P = t, -t < 0.4$; $P = -0.52, -t > 0.4$ (dotted line Fig. 5) was used. Above neutron momenta of $\sim$ 2.75 GeV/c, CE $n-p$ becomes the dominant contributor to the FoM. This simple ROOT-based MC model gives detection-efficiencies consistent with those calculated in Geant-4.

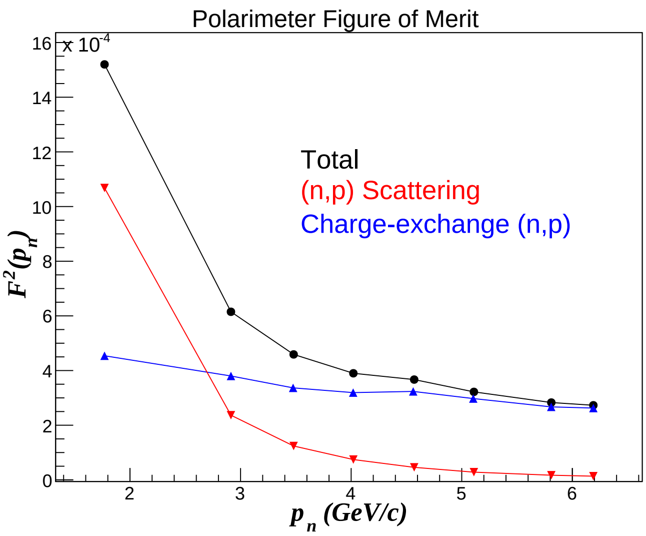

Figure 6: Neutron polarimeter figure of merit as a function of incident neutron momentum. Red: standard $n-p$ scattering, blue: charge-exchange $n-p$ scattering, black: sum of the two scattering channels.

3 Experimental Method

The recoil polarization technique requires a large number of counts, because of the relatively low analyzing power of the polarimeter. Going to high momentum transfer, where the elastic scattering rate scales approximately as $E^2_{\mathrm{beam}}/Q^{12}$, requires high luminosity, large acceptance and a high rate capability in the

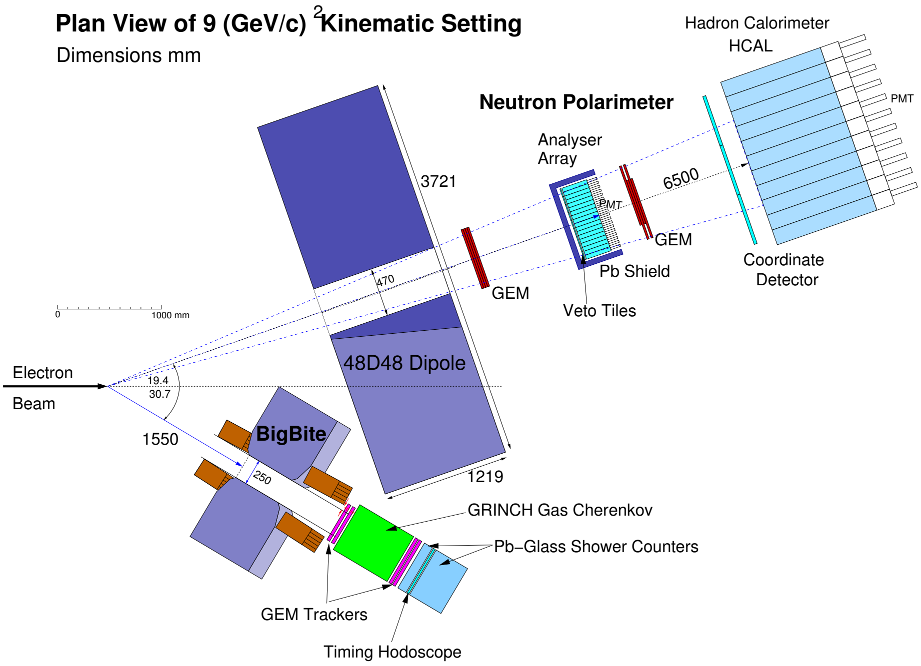

Figure 7: Plan view of experiment $Q^2 = 9$ (GeV/c)^2.

detection system. A plan view of the detector apparatus is displayed in Fig.7.

We propose to perform the measurement in Hall-A of Jefferson Laboratory, using the CW, polarized electron beam from the CEBAF accelerator. This will have a maximum energy of 11 GeV and maximum current of 80 μA. The present experiment will use beam energies 2.2, 4.4, 6.6 and 8.8 GeV (Table 1) integral factors of a the standard 2.2 GeV energy gain per pass. Beam polarizations in excess of 80% have been achieved routinely during 6 GeV operation of CEBAF and 80% is assumed for estimates of precision in measuring form factor ratios.

The electrons will be incident on a 10 cm long liquid deuterium (LD_2) target with 100 μm Al entrance and exit windows, giving ~ 0.054 g/cm^2 of material, compared to ~ 1.69 g/cm^2 for the LD_2. A liquid hydrogen (LH_2) target will also be used for calibrations. A 40 μA electron beam incident on a 10 cm LD_2 target produces an electron-neutron luminosity of $\sim 1.26 \times 10^{38}$ cm^{-2}s^{-1}.

Scattered electrons are detected in the BigBite spectrometer, which will reconstruct the momentum, direction and reaction vertex, as well as correlating the trigger time to an accelerator beam bunch . The neutron arm will be a polarimeter which consists of a plastic scintillator analyzer array, equipped with charged-particle veto tiles, followed by a GEM tracker and the hadron calorimeter HCAL. The polarimeter will provide position and time-of-flight information for the recoiling nucleon, as well as scattering asymmetries. Neutron spin precession will be performed by the "48D48" dipole which is the basis of the SBS charged-particle spectrometer. The experimental components are described in more detail in the following subsections.

3.1 The e' Spectrometer BigBite

BigBite is a large-acceptance, non-focusing magnetic spectrometer which, when positioned with the entrance aperture of the dipole 1.55 m from the target center, subtends a solid angle of $\sim$ 58 msr. BigBite is equipped with lead glass pre-shower and shower counters to provide a trigger which is insensitive to low energy background. In conjunction with the "GRINCH" Cherenkov, these counters distinguish electrons cleanly from π^-. Event timing is performed by a plastic scintillator hodoscope consisting of 90 $600 \times 25 \times 26$ mm bars of EJ200 plastic. Tracking is performed by three 400×1500 mm Gas Electron Multiplier (GEM) chambers at the front, followed, after a flight path of $\sim$ 650 mm (where GRINCH is located), by three 600×2000 mm GEM chambers. The GEM trackers supersede the MWDC, used in pre-upgrade experiments, and offer increased counting rate capability, so that higher luminosities may be achieved. They will be assembled from the 400×500 mm and 500×600 mm modules which are being constructed for the SBS program of experiments. The forward GEM will have a position resolution $\sigma_r \sim 70$ μm (60 μm has been obtained from prototype tests) and the two groups of trackers are separated by around 0.65 m. The angular resolution may estimated from

$$\delta\theta = \sqrt{\left(\frac{\sigma_r}{z_{tr}}\right)^2 + \left(\frac{13.6}{\beta c p_e}\sqrt{\frac{x}{X_0}}\left[1 + 0.038 \ln\left(\frac{x}{X_0}\right)\right]\right)^2} \tag{13}$$

where p_e is the electron momentum in MeV/c and x/X_0 is the thickness of intervening material in radiation lengths. This translates to an angular resolution of $\sigma \sim 1$ mr in both dispersive and non-dispersive directions. For the relatively small deflection obtained with an integrated field strength of 1.2 Tm and electrons of 1–3.5 GeV/c, the angle of deflection is given by:

$$p_e \approx \frac{e \int B.dl}{\theta} \tag{14}$$

The momentum resolution of $\delta p/p \sim 0.5\%$ will be adequate for the present experiment (Sec.3.5). The z-vertex resolution at the target is around 4 mm. It is extremely important to have an accurate knowledge of the vertex and four-momentum of the virtual photon, so that the BigBite optics and vertex reconstruction will be calibrated at each kinematic setting, using a sieve slit and multi-carbon-foil target. Momentum will be calibrated using elastic *ep* scattering from a LH_2 target.

Timing from BigBite is provided by a plastic scintillator hodoscope. For high luminosity operation a new, finer granularity, hodoscope is being constructed. This will consist of 90 plastic scintillator elements, each $25 \times 25 \times 600$ mm, each read out by 2, ET9142 photomultipliers (PMT). The intrinsic timing resolution of this device, measured with cosmic-ray muons, is 0.1 ns.

Offline charged particle identification is aided by the "GRINCH" threshold gas Cherenkov. Light is collected by a cylindrical mirror and reflected on to a set of 510 9125 PMT's. Compared to a previous gas Cherenkov, which used 5" PMTs, the new detector will have superior counting rate capability and will be much less susceptible to soft background from the electron beam line.

3.2 The Neutron Polarimeter

The neutron polarimeter (Fig. 7) consists of five main components:

1. An array of plastic scintillator blocks acts as an active polarization analyzer.
2. The segmented hadron calorimeter HCAL, which is optimized to detect nucleons with momenta of 1.5 - 10 GeV/c with high efficiency.
3. An array of plastic scintillator veto tiles, sited directly in front of the analyzer provide charged particle identification.
4. A set of GEM chambers situated between the analyzer and HCAL
5. The coordinate detector situated between the GEM tracker and HCAL.

3.2.1 The Plastic Scintillator Analyzer Array and Veto Detector

The analyzer consists of a 18×48 array of $40 \times 40 \times 250$ mm bars of EJ-200 plastic scintillator, aligned with their long axes parallel to the incident neutrons. Each bar will be read out by a 28 mm ETL 9125 PMT, attached on the downstream side of the bar, which will give an estimated time resolution of 0.9 ns FWHM. A set of 1 cm thick plastic scintillator "veto tiles" placed directly in front of the analyzer aids identification of incident charged particles. A finely segmented analyzer is obviously desirable in terms of its position resolution and counting rate. The 40×40 mm cross section represents a reasonable compromise in terms of cost and compatibility with the available PMT's. Counting rates in the analyzer are discussed in Sec.3.4.

The response of the analyzer array to incident 4 GeV/c neutrons has been simulated and the resulting data analyzed to give the position resolution and neutron detection efficiency. This has produced an uncertainty in reconstructed neutron polar angle $\delta\theta_n = 0.17^\circ$ which increases to 0.18° if a 50 mm thick Pb wall is placed before the analyzer (and the veto layer is employed to veto charged particles produced by conversion of neutrons in the Pb). The detection efficiency, the fraction of incident neutrons which register a hit in the analyzer, has a value of 21.2% when a detection threshold of 20 MeV is applied. With the Pb wall in place and the veto-tile anti coincidence requirement, the effective efficiency is reduced slightly to 19.1%.

3.2.2 The GEM Charged Particle Tracker

The analyzer is followed by a tracker of the charged particles produced by CE $n-p$ scattering or non-elastic processes within the analyzer. This increases the information obtained on the various reaction processes within the analyzer. It is constructed from 500×600 mm GEM modules of the same type used in the GEp(5) polarimeter [3]. In the event that a precise calibration of reconstructed scattering angles in the polarimeter using protons is necessary, an additional set of trackers will be installed in front of the analyzer array. The GEM based trackers will have very high counting rate capability. Compared to GEp(5) the present experiment will run at a factor ~ 10 lower luminosity and the polarimeter will sit at more backward angles. Thus we anticipate that the GEM chambers will handle the lower background rates comfortably.

3.2.3 The HCAL Hadron Calorimeter

Downstream of the tracker comes a 12×24 array of $150 \times 150 \times 1000$ mm calorimeter modules (HCAL) which are formed from a sandwich of Fe and plastic scintillator plates. Scintillation light is collected on a wavelength-shifting guide and then piped to a PMT. The time resolution of prototype modules is around 300 ps for cosmic-ray muons.

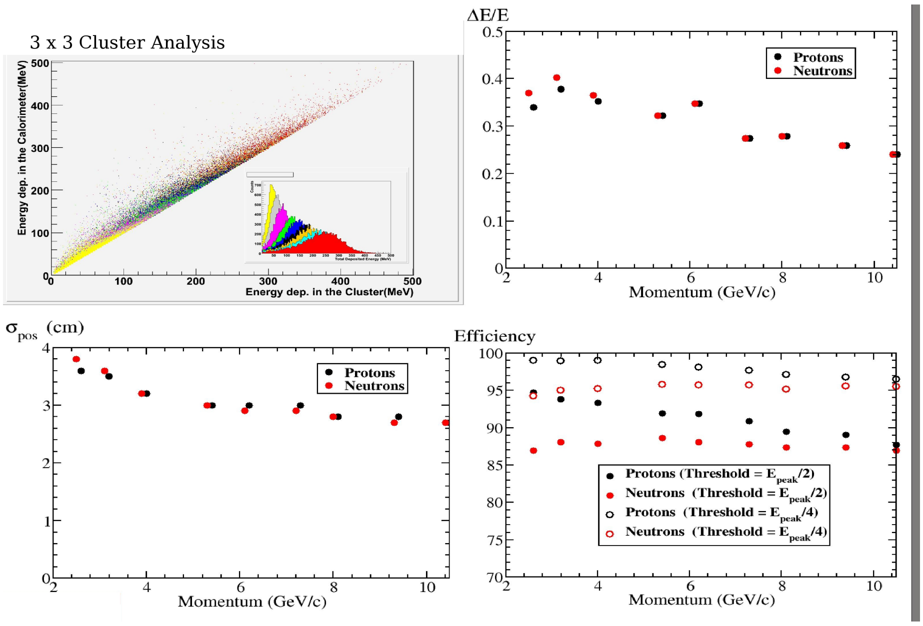

Figure 8: Calculations of HCAL response. Top left: energy leakage from a 3×3 hit cluster; top right: fitted energy resolution of the peak region of the pulse height response; bottom left: position resolution from cluster mean position; bottom right: detection efficiency for 2 threshold settings.

The simulated response of the HCAL response are displayed in Fig. 8 and is very similar for neutrons and protons. The peaked pulse-height response means that thresholds can be set high to suppress low energy background from the experimental trigger, without large reductions in detection efficiency. A position resolution of around 30 mm results in a resolution for the reconstructed scattering angle of around 12 mr, which sufficient for selection of "good" scattering angles where the analyzing power is high (Sec. 2.1.1). In the case of CE $n-p$ scattering the rear set of GEM chambers will provide the primary information on angle.

3.2.4 Rear Detector for Charged-Particle Identification

A "coordinate detector" (CD), based on $3 \times 30 \times 1000$ mm plastic scintillator strips, is under design for use on the electron arm of the GEp(5) experiment [3].

There the CD would be used in conjunction with an electromagnetic calorimeter to identify electrons and provide good hit-coordinate resolution. The CD modules would also be suitable for this experiment, where the electron-arm spectrometer is BigBite, and would be placed before HCAL to differentiate charged from neutral particles scattering from the analyzer.

The CD readout will be by 2 mm WLS optical fibers, connected to multi-anode PMTs, which have been procured from FNAL. The projected time resolution is ~ 0.5 ns, which will allow tight coincidence conditions to be made between the CD, the Analyzer array and HCAL. The efficiency of one CD layer is around 92% for minimum-ionizing particles and the rate capability will be high, to function effectively in the much higher luminosity GEp(5) experiment.

3.2.5 The 48D48 Dipole

For quasi-elastic neutron detection the dipole (known as 48D48) has no direct use as a spectrometer, but it serves several purposes:

1. To precess the longitudinal component of spin of the recoiling neutron to the vertical direction as the nucleon polarimeter measures transverse components of spin only.
2. To deflect protons produced in quasi-elastic $^2\mathrm{H}(\mathrm{e},\mathrm{e}'\mathrm{p})$. These are then separated from quasi-elastic neutrons through angular correlations with the $\vec{q}$ vector determined from the electron arm. Preliminary calculations suggest that a ~ 2 Tm integrated field will produce clean $n-p$ separation at incident nucleon momenta up to ~ 5 GeV/c.
3. To sweep low-momentum, charged background out of the acceptance of the polarimeter. For an integrated field strength of 2 Tm, all charged particles with momenta below $\sim$0.78 GeV/c are swept beyond the Analyzer acceptance.

Neutron spin precession through the dipole field has been calculated using the Geant-4 polarimeter model. Non-perpendicular incidence with respect to the field direction, e.g. due to fringe fields and an extended angular range, produces small rotations in the $z-x$ plane which can affect P_x/P_z and hence $\mathrm{G_E}/\mathrm{G_M}$.

The 48D48 dipole, is currently being modified for use in Hall A, and thus a field measurement is not yet available. However, we have calculated the size of possible $z-x$ mixing effects using field maps obtained using the 3D code TOSCA [51]. The employed field map calculation did not include any field clamps and thus represents a worst-case scenario in terms of the stray field, which extends beyond the confines of the dipole aperture. At a coil excitation of ~ 2000 A, an integrated field strength of ~ 2 Tm is calculated, which produces a spin rotation $z \to y$ of $\sim \pi/2$. Neutrons with an initial polarization $\mathbf{P} = (0,0,1)$ and a momentum of 3 GeV/c were tracked through the dipole field and their polarization recorded when they impinge on the analyzer. The value of P_x, calculated after passing through the field, is at the few % level and varies smoothly as a function of the hit position. If the maximum degree of spin transfer $z \to x$ is ~ 0.05 and the expected ratio P_x/P_z in a $\mathrm{G_E^n}/\mathrm{G_M^n}$ measurement is ~ 0.2, then the maximum error induced in a measurement of P_x/P_z will be

$\sim$ 25%. Given that the analyzer will have a position resolution of $\sim$ 1 cm, and the maximum gradient $\delta P_x/\delta x$ is $\sim 0.005/cm$, the maximum error after correction will be $\sim$ 2.5%. The size of the effect, integrated over the angular acceptance of the SBS dipole, will be considerably smaller.

3.3 Kinematics

Kinematic settings have been calculated for $\mathrm{Q}^2 = 2.0,\ 4.0, 6, 9\ (\mathrm{GeV/c})^2$ and are summarized in Table 1. The nominal "central" values of the momenta and angles relate to free $n(e, e'n)$.

Setting	Q^2 (GeV/c)^2	E_e (GeV)	$p_{e'}$ (GeV)	θ_e (deg.)	θ_n (deg.)
1	2.0	2.2	1.14	52.8	31.1
2	4.0	4.4	2.24	37.3	27.5
3	6.0	6.6	3.40	30.0	25.0
4	9.3	8.8	3.81	30.7	19.4

Table 1: Kinematic Settings. Elastic n(e,e'n) central values

The ranges of kinematic variables for the nominal settings of the large acceptance detector system were calculated for quasi-free $^2\mathrm{H(e,e'n)}$, where the internal momentum distribution of the neutron was sampled from $p_N^2 . \exp(-p_N^2/2\sigma_N^2)$, $\sigma_N = 0.03$ GeV/c, i.e. the Fermi momentum distribution was approximated by a Gaussian of width 0.03 GeV/c. Events were generated along the 10 cm length of the target and scattered electrons were detected within the effective 250×750 mm aperture of BigBite situated $\sim$ 2 m from the target center. It was also checked if the recoiling neutron is within the acceptance of the 48D48 aperture. BigBite subtends a solid angle of $\sim$ 58 msr and more than 91% of correlated neutrons pass through the aperture of the 48D48 at all settings. Fig. 9 (left) displays the calculated coverage in Q^2 while the BigBite angular acceptance (middle) and corresponding $^2\mathrm{H(e,e'n)}$ neutron acceptance (right) are shown in Fig.9 for kinematic setting 4 of Table 1.

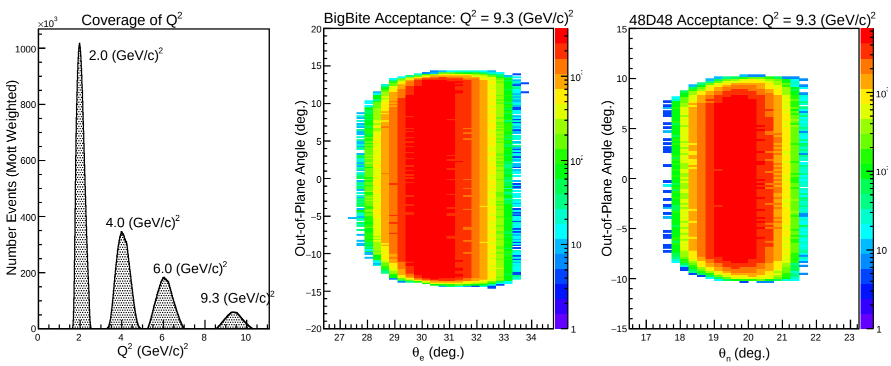

Figure 9: Left: range of Q^2 for the nominal settings labeled on the plot. The distributions are weighted by the Mott cross section. Middle: electron angular coverage of BigBite. Right: neutron angular coverage of the 48D48 dipole.

3.4 Background Rates and the Trigger Rate

Preliminary singles rates in detectors have been evaluated using the code DINREG [52], which is well proven in estimating background rates in Hall-A. At the setting pertinent to $Q^2 = 4$ (GeV/c)^2: $E_{beam} = 4.4$ GeV, $\theta_{e'} = 37.3°$, $\Omega_{e'} = 58$ msr, $\mathcal{L}_n = 1.3 \times 10^{38}\text{cm}^{-2}\text{s}^{-1}$, the BigBite trigger rate is estimated at ~ 50 kHz, of which 5_kHz is from charged particles and 45 kHz from uncharged (π^0). Thus a coincidence with the neutron arm will be desirable for triggering purposes. Equivalent calculations for the neutron arm detectors, made with an integrated field strength of 1.7 Tm which will sweep charged particles of momenta $\lesssim 650$ MeV/c out of the analyzer acceptance. The estimated rate in individual analyzer bars, for a threshold of 5 MeV, will be ~ 0.1 MHz, which is well within the capabilities of a fast plastic scintillator. The combined rate in a 4×4 cluster of HCAL modules, for incident neutrons of ~ 3 GeV/c and a trigger threshold of 1/2 of the peak value in the pulse height distribution, is estimated to be 100 kHz. This translates to a total rate of 1.5 MHz in the calorimeter.

With 50 kHz in BigBite, 1.5 MHz from HCAL and a coincidence window of 50 ns, the accidental rate will be ~ 4 kHz. This may yet prove to be uncomfortably high for the DAQ system. With improved fast photon-electron selection in the BigBite trigger, the rate would be reduced significantly. We will investigate the effect of the BigBite GRINCH Cherenkov on trigger decisions.

3.5 Inelastic Background Rejection

Inelastic processes, largely associated with pion electroproduction and quasi-elastic $^2H(e, e'p)$, constitute potential sources of background to the quasi-elastic $^2H(e, e'n)$ signal. Contamination of the electron-arm, quasi-elastic (QE) event sample by charged pions is expected to be extremely small. Background processes such as pion photoproduction will be suppressed very effectively by offline cuts and should not constitute a significant source of contamination. For the nucleon momenta of interest here, QE neutrons may be separated cleanly from the equivalent protons, which are deflected by the 48D48 dipole magnet before incidence on the polarimeter (Sec.3.2.5).

It is expected that the present experiment, using a ^{2}H target will have significantly better separation of the QE signal than experiments which employ a ^{3}He target. The present experiment is similar in many respects to experiment E12-09-019 to measure $\text{G}_\text{M}^\text{n}/\text{G}_\text{M}^\text{p}$ [2], which also employs BigBite on the electron arm and the HCAL array on the nucleon arm. It is expected that the momentum and angle resolutions are going to be very similar. In E12-009-019 the QE signal has been modeled in a similar way to the present calculations, while inelastic background was calculated using code Genev [54], smeared by Fermi motion and detector resolution. Some of these calculations at $Q^2 = 3.5$ (GeV/c)^2 are shown in Fig. 10 (Top). Here the acceptance averaged cross section is plotted against W^2 and θ_{qn}, the angle between the direction of the virtual photon and the direction of the recoiling neutron. The estimated systematic uncertainty in subtracting background from the QE signal is estimated to be $\sim 2\%$.

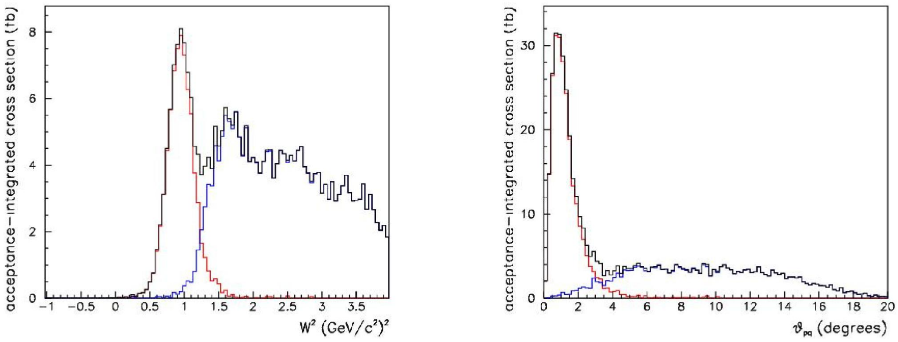

Figure 10: Top panels: Separation of quasi-elastic and inelastic events for $d(e, e'n)$ events at $\mathrm{Q}^2 = 3.5\ (\mathrm{GeV/c})^2$ from experiment E12-009-019 [2]. The QE signal is in red, inelastic background in blue and total in black.

3.6 Systematic Uncertainties

Potential sources of experimental systematic error are :

- Beam polarization uncertainty, which cancels in a ratio measurement.
- Analyzing power uncertainty, which cancels in a ratio measurement.
- Azimuthal angle acceptance non-uniformity, which cancels after beam helicity flip and the additional check of precession angle flip.
- Variation in the effective analyzing power with azimuthal angle. Preliminary calculations do not show any significant variations. However, potential variations in the effective analyzing power, which may be different in the x and y directions, as one scans over the full vertical and horizontal range of the analyzer, are not ruled out. If this proves to be a significant effect, then it can be corrected using the good position resolutions of the analyzer and HCAL arrays.
- Separation of P_x from P_z does not rely on variation of the magnitude of the spin-precession magnetic field. In the present experiment P_x and $P_z(P_z \to P_y)$ are measured simultaneously with the same precession field, so that potential effects of changes to the background counting rates on the measured asymmetry are thus avoided. Non-uniformity of the magnetic field results in a small amount of $P_z \to P_x$ mixing. Given that the analyzer array has good position resolution, the neutron path through the dipole can be reconstructed accurately and this this effect corrected with an overall uncertainty of 1%.
- Reproducibility of the spin precession angle after polarity reversal. At a precession angle of $\sim 75\%$, a 1% difference in integrated field would give 0.25% difference in $P_z \to P_y$.
- The vertical distribution of counting rates in the polarimeter will change when the polarity of the spin precession dipole is reversed. Any significant effect from changes to the level of signal contamination will show up when

different combinations of beam-helicity-flip and dipole-flip asymmetries are compared.

- Variation in the angle of spin precession through the dipole magnet. The path of a neutron through the dipole can be reconstructed with sufficient precision that a correction factor can be evaluated event by event. The estimated uncertainty is 0.25%.
- Dilution of the asymmetry by accidental background. The background is estimated to be at the 1% level (Sec.3.4) which can be subtracted without significant error.
- Contamination of the quasi-elastic signal by inelastic processes. A deuteron measurement will have cleaner rejection of the inelastic background. An estimate of 2% is made (Sec. 3.5), based on comparison with background estimates from experiment E12-009-019 and Monte Carlo calculations of the present QE signal.
- Dilution of the asymmetry, due to proton charge exchange (mainly in the Pb shield) upstream of the veto detectors of the analyzer array. This factor may be evaluated using data from ^{1}H, ^{3}He and ^{12}C targets. In GEn(1) the associated systematic uncertainty was between 3 and 4%. Here protons will be deflected by a dipole magnet before interaction in the Pb wall and thus resultant neutrons will tend to be displaced outside of quasi-elastic data cuts. We estimate a 1% uncertainty provisionally.

Overall we estimate that a 3% systematic error is achievable.

4 Estimates of Experimental Uncertainty

The estimate of experimental uncertainty in the ratio $R = G_E^n/G_M^n$ is based on the following:

1. The expected degree of polarization of the incident electrons. Previous measurements indicate that values in excess of 0.8 are generally available and we use the value 0.8 for the following estimates.
2. The acceptance of BigBite and the polarimeter for quasi elastic $^2\mathrm{H}(\mathrm{e},\mathrm{e}'\mathrm{n})$. The kinematic settings are given in Sec.3.3.
3. The predicted detection efficiency and acceptance of the polarimeter is based on Monte Carlo studies. The overall efficiency of the polarimeter, after scattering angle selection, is around 7%.
4. The estimate of the $n + \mathrm{CH}$ analyzing power has been obtained using the procedure described in Sec.2.1.1. The polarimeter figure of merit $\mathcal{F}^2$ has been obtained from a Monte Carlo evaluation of Eq.11, and the uncertainty in polarization from Eq.12.

Table 2 displays parameters relevant to the precision of the polarization measurement for neutron momenta (p_n^{lab}) associated with the present kinematic settings (Table 1). The counting rate and polarization uncertainty estimate (Table

Q^2 (GeV/c)^2	p_n^{lab} GeV/c	P_eP_x	P_eP_z	$\mathcal{F}^2$ $\times 10^{-4}$
2.0	1.72	0.157	0.635	15.2
4.0	2.89	0.175	0.549	6.1
6.0	3.97	0.176	0.508	3.9
9.3	5.82	0.189	0.551	2.8

Table 2: Mean values of polarization parameters at the kinematic settings of the present proposal.

Q^2	$\Omega_{e',n}$	$\sigma_n(\theta)$	Rate	Time	δP	$\delta R/R$	
(GeV/c)^2	(msr)	(pb/sr)	(Hz)	(hr)	$\times 10^{-3}$	(stat)	(sys)
2.0	58.1	151	1109	24	3.70	0.024	0.03
4.0	55.8	17.4	122	48	12.4	0.075	0.03
6.0	53.7	4.23	28.6	150	18.2	0.110	0.03
9.3	58.6	0.43	3.17	750	28.7	0.160	0.03

Table 3: Counting rate and error estimate for $^2H(\vec{e},e'\vec{n})$ at an incident (neutron) luminosity of 1.26×10^{38} cm^{-2}s^{-1}. "Rate" is the mean $n(e,e'n)$ rate incident on the analyzer, δP is the statistical uncertainty in the polarization and $\delta R/R$ is the relative uncertainty in the ratio $R = G_E^n/G_M^n$.

3) is based on the expected luminosity and the cross section for free $\mathrm{n(e,e'n)}$ scattering. The cross section and P_x, P_z polarization values have been calculated using a parametrization of the Q^2 dependence of the Sachs form factors [53].

5 Summary and Comparison with other G_E^n/G_M^n measurements at Jefferson Lab.

Q^2 (GeV/c)^2	1.5	2.0	3.7	4.0	6.0	6.8	9.3	10.2
E12-09-016 stat.	0.003	–	0.018	–	–	0.073	–	0.090
E12-09-016 sys.	0.005	–	0.013	–	–	0.027	–	0.026
Beam Time (hr)	24	–	48	–	–	96	–	744
This LOI stat.	–	0.008	–	0.038	0.067	–	0.125	–
This LOI sys.	–	0.008	–	0.010	0.011	–	0.012	–
Beam Time (hr)	–	24	–	48	150	–	750	–

Table 4: A comparison, between this LOI and experiment E12-09-016, of the estimated statistical and systematic uncertainties δR ($R = \mu_n G_E^n/G_M^n$), obtained for the displayed beam times. The estimates use the Galster parametrization [55] for G_E^n and the Kelly parametrization [18] for G_M^n

We propose to measure the ratio $\mathrm{G_E^n/G_M^n}$ from a double-polarization asymmetry, using the longitudinally polarized CEBAF electron beam and a polarimeter to measure the transfer of polarization to the recoiling neutron in

Q^2 (GeV/c)^2	2.0	4.0	6.0	6.9	9.3
E12-11-009 stat.	–	0.101	–	0.163	–
E12-11-009 sys.	–	0.03	–	0.03	–
Beam Time (hr)	–	240	–	720	–
This LOI stat.	0.024	0.071	0.094	–	0.151
This LOI sys.	0.03	0.03	0.03	–	0.03
Beam Time (hr)	24	48	150	–	750

Table 5: A comparison, between this LOI and experiment E12-11-009, of the estimated relative statistical and systematic uncertainties $\delta G_E^n/G_E^n$ obtained for the displayed beam times. The estimates use the BLAST parametrization [53] to the Sachs form factors.

quasi-elastic $^2\mathrm{H}(\vec{e}, e^{'}\vec{n})$. The measurement will be made at four values of the squared four-momentum transfer of the scattered electron: $\mathrm{Q}^2 = 2.0$, 4.0, 6.0, and 9.3 (GeV/c)^2. The Jefferson Lab. PAC has previously approved two experiments to measure $\mathrm{G_E^n/G_M^n}$, but each has used a different procedure to present the uncertainties and these differences affect the estimated size of the error bars.

- E12-09-16 [1] has calculated the Sachs form factors using the Galster parametrization [55] for G_E^n and the Kelly parametrization [18] for G_M^n and presented the uncertainties δR ($R = \mu_n G_E^n/G_M^n$).
- E12-11-009 [36] has calculated G_E^n and G_M^n using the "BLAST" parametrization [53] and presented the uncertainty $\delta G_E^n/G_E^n$.

We have evaluated the uncertainties of the present experiment using both prescriptions and compare these separately to E12-09-16 (Table 4, Fig.11) and to E12-11-009 (Table 5).

Compared to the polarized ^{3}He target experiment E12-09-16, the present experiment does not achieve quite as high precision, but on the other hand the systematic uncertainties associated with the $^2\mathrm{H}(\overrightarrow{e}, e^{'}\overrightarrow{n})$ technique are smaller than for $\overrightarrow{^3\mathrm{He}}(\overrightarrow{e}, e^{'}n)$. Using an ^{2}H target, separation of the quasi-elastic signal from inelastic background is much cleaner than for ^{3}He.

Experiment E12-11-009 uses the same $^2\mathrm{H}(\overrightarrow{e}, e^{'}\overrightarrow{n})$ method as this experiment, but in a similar measurement time the present experiment would produce significantly higher precision over a much broader range of Q^2. This is primarily due to differences in the design of the neutron polarimeters. The present device has large acceptance both for $n-p$ scattering and charge-exchange $n-p$, while the E12-11-009 device has significant acceptance only for $n-p$. As discussed in Sec. 2.1.1, charge-exchange $n-p$ offers much higher analyzing power at neutron momenta $p_n \gtrsim 3$ GeV/c and thus opens the possibility to make precise measurements at high Q^2 in a reasonable time.

Experiments to measure $\mathrm{G_E^n/G_M^n}$ are extremely challenging and it is important that the results can be verified using different experimental techniques with different systematic effects. In this respect the present experiment matches the Q^2 range and precision of E12-09-16 closely and together these experiments

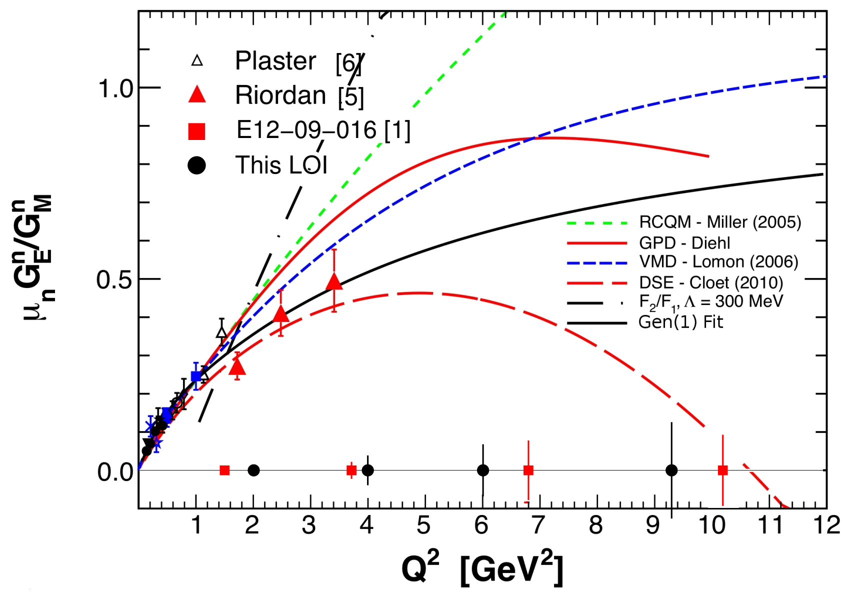

Figure 11: A comparison of the uncertainties of this LOI (black circles) with those of E12-09-016 [1] (red squares).

will provide the data to confront the latest theoretical developments in non-perturbative QCD.

If this LOI receives a favorable response from PAC 43, then we plan to submit a full proposal in 2016. Towards this, we plan to explore further the possibility to reach high Q^2 using the present experimental approach, and also an alternative which employs a passive polarimeter analyzer, similar to that of GEp(5) [3].

References

[1] *Measurement of the Neutron Electromagnetic Form Factor Ratio* G_E^n/G_M^n *at High* Q^2, JLab Experiment E12-09-016, Spokespersons: G. Cates, S. Riordan, B. Wojtsekhowski. *The Electric Form Factor of the Neutron with SBS*, S. Riordan, SBS Review, March 28, 2012.

[2] *Precision Measurement of the Neutron Magnetic Form Factor at to* $Q^2 = 18$ (GeV/c)^2. Jefferson Lab experiment E12-09-019, Spokespersons: J. Annand, R. Gilman, B. Quinn, B. Wojtsekhowski,

[3] *Large Acceptance Proton Form Factor Ratio Measurements at 13 and 15* (GeV/c)^2 *Using Recoil Polarization Method,* JLab Experiment E12-07-109, Spokespersons: E. Brash, E. Cisbani, M. Jones, C.F. Perdrisat, L.P. Pentchev, V. Punjabi, B. Wojtsekhowski.

[4] *Precision Measurement of the Proton Elastic Cross Section at High* Q^2, JLab. experiment E12-07-108, Spokespersons: J.Arrington, S. Gilad, B. Moffit, B. Wojtsekhowski.

[5] S. Riordan *et al.*, Jefferson Lab experiment E02-013, Phys. Rev. Lett. 105(2010), 262302.

[6] B. Plaster *et al.,* Phys. Rev. C73(2006), 025205., R. Madey *et al.*, Phys. Rev. Lett. 91(2003),122002.

[7] S.J. Brodsky, G.R. Farrar, Phys. Rev. D11(1975), 1309.

[8] M.K. Jones *et al.* Phys. Rev. Lett. 84(2000), 1398.

[9] O. Gayou *et al.*, Phys. Rev. Lett. 88(2002), 092301.

[10] V. Punjabi *et al.*, Phys. Rev. C71(2005), 055202.

[11] A.J.R. Puckett *et al.,* Phys. Rev. Lett. 104(2010), 242301.

[12] A. Puckett et al., Phys. Rev. C85(2012),045203.

[13] L. Andivahis *et al.*, Phys. Rev. D50(1994), 5491.

[14] M.E. Christy *et al.*, Phys. Rev. C70(2004), 015206.

[15] I.A. Qatten *et al.*, Phys.Rev.Lett. 94(2005), 142301.

[16] A.V. Belitsky, X. Ji and F. Yuan, Phys. Rev. Lett. 91(2003), 092003.

[17] B. Wojtsekhowski, Private Communication, Nov. 2010.

[18] J.J. Kelly, Phys. Rev. C70(2004), 068202.

[19] C.D. Roberts and A. G. Williams, Prog. Part. Nucl. Phys. 33(1994), 477.

[20] I.C. Cloët *et al.*, Few-Body Syst., 46 (2009), 1.

[21] J. Segovia *et al.*, Few-Body Syst. 55 (2014), 1185.

[22] D.J. Wilson *et al.*, Phys. Rev. C85(2012),025205.

[23] G.D. Cates, C.W. De Jager, S. Riordan and B. Wojtsekhowski, Phys. Rev. Lett. 106(2011), 252003.

[24] I.Cloet et al., Phys. Rev. C 90, (2014), 045202.

[25] M.Diehl and P.Kroll, Eur. J. Phys. C73 (2013), 2397.

[26] I. Passchier *et al.*, Phys. Rev. Lett. 82(1999), 4988.

[27] H. Zhu. Phys. Rev. Lett. 87(2001), 081801.

[28] J.Becker *et al.*, Eur. J. Phys. A6(1999), 329.

[29] D.Rohe *et al.*, Phys. Rev. Lett. 83(1999), 4257.

[30] B.S. Schlimme, Proc. SPIN2010, J. Phys.: Conf. Ser. 295 (2011), 012108.

[31] T. Eden *et al.*, Phys. Rev. C50(1994), 1749.

[32] C. Herberg *et al.*, Eur. J. Phys. A5(1999), 131.

[33] M. Ostrick *et al.*, Phys. Rev. Lett. 83(1999), 276.

[34] D.I. Glazier *et al.*, Eur. J. Phys. A24(2005), 101.

[35] G. Warren *et al.*, Phys. Rev. Lett. 92(2004), 042301.

[36] *The Neutron Electric Form Factor at* Q^2 *up to* 7 $(\mathrm{GeV/c})^2$ *from the reaction* $^2\mathrm{H}(\overrightarrow{e},\mathrm{e}'\overrightarrow{n})$ *via Recoil Polarimetry.* JLab. Experiment E12-11-009, Spokespersons: B.D. Anderson, J. Arrington, S. Kowalski, R. Madey, B. Plaster, A. Yu. Semenov. *E12-11-009 (G_{En}) Update,* M. Kohl, Hall C Users Meeting, Feb. 21-22, 2014.

[37] A.I. Akhiezer *et al.*, JEPT 33(1957), 765.

[38] R.G. Arnold *et al.*, Phys. Rev. C23(1981), 36.

[39] N.V. Vlasov *et al.*, Instr. and Exp. Tech. 49(2006), 49.

[40] *Measurement of analyzing powers for the reaction* $p + CH_2$ *up to 7.5 GeV/c and* $n + CH$ *up to 4.5 GeV/c at the Nuclotron,* ALPOM2 proposal to JINR Dubna PAC, March 2015, Spokespersons: N.M. Piskunov, C.F. Pedrisat, V. Punjabi, E. Tomasi-Gustafsson.

[41] R. Diebold *et al.*, Phys. Rev. Lett. 35(1975), 632.

[42] S.L. Kramer *et al.*, Phys. Rev. D17(1978), 1709.

[43] H. Spinka *et al.*, Nucl. Instr. and Meth. A211(1983), 239.

[44] L.S. Azhgirey *et al.*, Nucl. Instr. and Meth. A538(2005), 431.

[45] N.E. Cheung *et al.*, Nucl. Instr. and Meth. A363(1995), 561.

[46] I.G. Alekseev *et al.*, Nucl. Instr. and Meth. A434(1999), 254.

[47] P.R. Robrish et al., Phys. Lett. B31 (1970), 617.

[48] M.A. Abolins et al., Phys. Rev. Lett. 30 (1973), 1183.

[49] CNS Center for Nuclear Studies, SAID Partial Wave Analysis, R. Arndt et al., http://gwdac.phys.gwu.edu/.

[50] *Analyzing Power of pp and np Elastic Scattering at Momenta between 2000 and 6000 GeV/c and Polarimetry at LHE*, V.P. Ladygin, JINR report E13-99-123, 1999.

[51] TOSCA/Opera-3D, Vector Fields Software, Cobham Technical Services, Dorset, UK

[52] P.V. Degtyarenko, computer code DINREG, *Applications of the Photonuclear Fragmentation Model to Radiation Protection Problems*, Proc. Second Specialist Meeting on Shielding Aspects of Accelerators (SATIF2), CERN, October 1995.

[53] E. Geis *et al.*, Phys. Rev. Lett. 101(2008), 042501.

[54] M. Ripani and E.M. Golovach, Program Genev, INFN Genoa 1994. Based on P. Corvisiero et al., Nucl. Instr. and Meth. A346 (1994), 433

[55] S. Galster *et al.*, Nucl. Phys. B32 (1971), 221.